

## Supporting materials for

### **Magnetic Carbon Nanostructures: Microwave Energy – Assisted Pyrolysis vs Conventional Pyrolysis**

Jiahua Zhu, Sameer Pallavkar, Minjiao Chen, Narendranath Yerra, Zhiping Luo, Henry A. Colorado, Hongfei Lin, Neel Haldolaarachchige, Thomas C. Ho,<sup>a</sup> David P. Young, Suying Wei\* and Zhanhu Guo\*

<sup>a</sup>Integrated Composites Laboratory (ICL), Dan F Smith Department of Chemical Engineering, Lamar University, Beaumont, TX 77710 USA. Tel: 1-(409)880-7654; E-mail: [zhanhu.guo@lamar.edu](mailto:zhanhu.guo@lamar.edu).

<sup>b</sup>Department of Chemistry and Biochemistry, Lamar University, Beaumont, TX 77710 USA, Tel: 1-(409) 880-7976; E-mail: [suying.wei@lamar.edu](mailto:suying.wei@lamar.edu).

<sup>c</sup>Department of Chemistry and Physics and Southeastern North Carolina Regional Microanalytical and Imaging Consortium, Fayetteville State University, Fayetteville, NC 28301 USA

<sup>d</sup>Department of Materials Science and Engineering, University of California Los Angeles, Los Angeles, CA 90095 USA

<sup>e</sup>Department of Chemical and Materials Engineering, University of Nevada Reno, Reno, NV 89557 USA

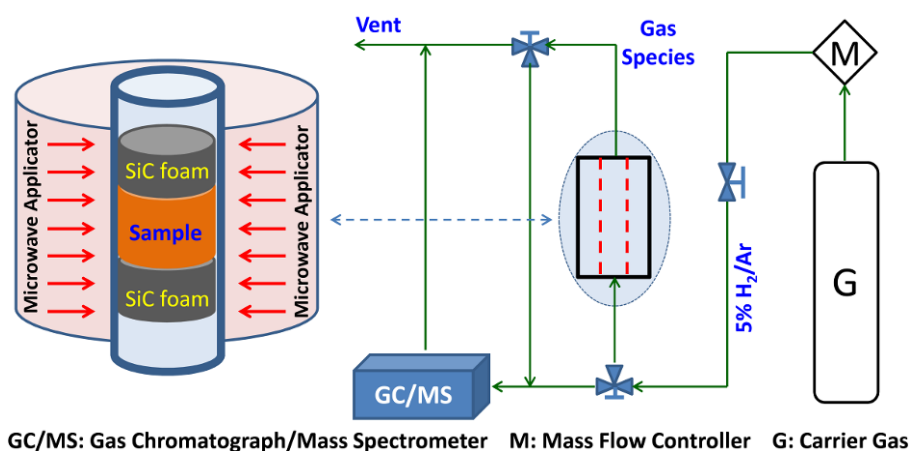
<sup>f</sup>Department of Physics and Astronomy, Louisiana State University, Baton Rouge, LA 70803 USA

## S1.1 Materials and nanocomposites preparation

The epoxy resin used is Epon 862 (bisphenol F epoxy) and EpiCure curing agent W, which are purchased from Miller-Stephenson Chemical Company, Inc. Core-shell structured Fe(core)@FeO(shell) nanoparticles (NPs), with a particle size of 15-25 nm and oxide thickness of 0.5 nm are provided by QuantumSphere, Inc. All the materials are used as received without any further treatment.

The detailed synthetic procedures of Fe@FeO/epoxy resin nanocomposites are described in our previous report.<sup>1</sup> Briefly, 20 wt% Fe@FeO NPs are weighed and then Epon 862 is added, keeping the mixture overnight until the surface of NPs is wetted completely. Then, the mixture is stirred at 400 rpm for 1 hour at room temperature. After that, Epicure curing agent W is added and further mechanically mixed (200 rpm) for 4 hours at a 70 °C water bath. The weight ratio of Epon 862 and Epicure W is 100:26.5 as recommended by the company. After removing the bubbles, the mixture is transferred to silicon-rubber molds and cured at 120 °C for 5 hours.

## S1.2 Microwave heating procedure



**Scheme S1** The schematic setup for the microwave annealing of epoxy nanocomposites and the consequent GC-MS analysis of the degraded gas species.

A schematic diagram of the experimental set-up is shown in Scheme S1. It consists of a gas cylinder, a mass flow controller, a packed bed reactor, a microwave generator, and a GC/MS for gas analysis. The packed bed reactor was a long quartz tube. It was packed with microwave absorbing material of silicon carbide (SiC) supported on glass wool, with the epoxy nanocomposite samples placed between the two SiC foams. The reactor was placed inside a microwave applicator, Scheme S1. The microwave heating unit was a research grade microwave heating system, which consists of a power supply, a microwave generator, a dummy load, a forward and reverse power detector, a tuner, and a terminator (sliding short circuit). The system was thoroughly examined and safe-guarded to ensure that no leaking of microwave occurred during experiments.

The carrier gas was controlled at a fixed flow rate by means of mass flow controller (Brooks instrument 5850-e series) and directed towards the packed bed system by means of a three-way control valve. The microwave absorbing media used was SiC foams (Hi-Tech Ceramics) with pore density of 80 ppi (pores per square inch), outer diameter being 10 mm and the length of each SiC foam being 2.5 cm, enclosed in a clear fused quartz tubing (Technical glass products Inc.) with inner diameter being 10.5 mm and its length being 30.48 cm. The used stack height of the packed bed was about 5 cm and the individual weight of the SiC foams used was about  $2.84 \pm 0.07$  grams. The inlet gases were fed to the applicator assembly using a ¼ inch Teflon tubing and the outlet gases were routed to the sampling system using ¼ inch 316 stainless steel tubing. Both ends were fixed using a ¼ inch Swagelok compression fitting. Once the microwave energy was irradiated at the SiC foams, the heated bulk surface temperature of these foams were measured using an infrared temperature measuring unit.

### **S1.3 Experimental procedure and temperature measurement**

The experimental procedure was carried out sequentially, with the first step being purging the packed bed media with an inert carrier gas such as N<sub>2</sub> (ultra high purity grade) at a controlled flow rate for about 20 minutes. Then, switching on the carrier gas of H<sub>2</sub>/Ar mixture (H<sub>2</sub> ~5% balanced with Ar) by means of a three-way valve, which was controlled by using a mass flow controller (Brooks Instrument Model 5850E series). This was followed by turning the cooling water supply on for the magnetron head and the short dummy load (Model No. GA1204, Gerling Applied Engineering Inc.). The data acquisition system (LabVIEW) was turned on to record bulk surface temperature of the packed bed reactor set-up (epoxy nanocomposites sandwiched between the two SiC foams), where the temperature was measured using the infrared temperature measuring unit (Mikron M90). This was followed by setting up the microwave power at the desired value and the microwave power source was then switched on. Immediately after switching on the microwave power source, both the forward and the reflected power were detected by their respective crystal detectors (Model No. GA3104/0015, Gerling Applied Engineering Inc.). The forward and the reverse microwave power were recorded by the dual microwave power meter (Model No. GA3004-2, Gerling Applied Engineering Inc.)

With the microwave power switched on, the energy's coupling with the enclosed absorbing media (packed bed reactor configuration) required the adjustment of the precision 3-Stub tuner to an expected power level (Model No. GA1009, Gerling Applied Engineering Inc.). This was achieved by adjusting the 3-Stub tuner for impedance tuning till the indicated value of the forward microwave power exceeded that of the reflected microwave power. Once hot surface temperature was achieved, the 3-Stub tuner was left

undisturbed for the entire duration of the experimental run which lasted for about 120 minutes. Off-gas samples were collected in the last 20 minutes of the experimental run in a gas sample bag, which was then diluted to about 5000 times using ultra high purity nitrogen as the dilution gas. The diluted gas sample was then analyzed off-line for speciation using the gas chromatography (Varian CP-3800) and the mass spectrometry (Saturn 2200) system. It is worth pointing out here that the gas sampling process during the last 20 minutes of the experimental run was carried out at a positive pressure, where excess gas sample was directed towards a bubbler (to ensure positive pressure) and then to the exhaust vent, so as to achieve in-situ gas samples during the annealing process.

As mentioned earlier, an infrared temperature measuring unit (Mikron M90) was used to measure bulk surface temperatures and its output signal was recorded using RS-232 data acquisition device (8-channel RS-232 device, National Instruments) and data acquisition software (LabVIEW). A temperature profile test was carried out, in which a controlled amount of carrier gas was fed through the applicator at ambient conditions for 120 minutes. Tests were carried out for different power levels and for different flow rate of carrier gas through the applicator.

The conventional annealing of the epoxy nanocomposites was conducted in a horizontal quartz tube and heated to 800 °C with a heating rate of 10 °C/min under the gas atmosphere of H<sub>2</sub>(5%)/Ar. The temperature was hold at 800 °C for 2 hours and then cooled down naturally.

#### **S1.4 Characterization**

The morphology of the core-shell nanoparticles was determined using a FEI Tecnai G2 F20 microscope with field emission gun, operated at an accelerating voltage of

200 kV. Samples for TEM observation were prepared by drying a drop of nanoparticles-ethanol suspension on the carbon-coated copper TEM grids.

***GC/MS for gas component analysis*** The collected gas samples were diluted by nitrogen gas (ultrahigh purity grade) in a Tedlar bag (SKC Inc., Part No. 232-05) with a dilution factor of 5000. The analytical tool used for the gas sample analysis was a gas chromatograph/mass spectrometer system (Varian CP-3800/Saturn 2200) with a built-in cryo-focus trap unit designed by Lotus Consulting Agency, to achieve detection capability in the parts per billion (ppb) range. Liquid nitrogen was used as the refrigerant to freeze the sample in the cryo-focus trap unit during the pre-concentration stage, with He (ultra high purity grade) as the purging gas.

The thermal stability of the core-shell nanoparticles was studied with a thermobalance (TGA, TA instruments TGA Q-500) from 25 to 900 °C with an air flow rate of 60 mL min<sup>-1</sup> and a heating rate of 10 °C min<sup>-1</sup>.

The Mössbauer spectrometer was set to produce a high precision Doppler velocity modulation of the source  $\gamma$  radiation. The effects of the Doppler velocity modulation on the absorption of  $\gamma$  radiation were recorded synchronously in the 1024 channels of the multichannel analyzer. The result was 1024 numbers representing registered gamma quanta (representing a singular quantum) passing through the absorber under the conditions of different Doppler velocity. A separate calibration procedure establishes the exact correspondent channel-velocity (the spectrometer calibration is performed by measuring a standard  $\alpha$ -Fe absorber, which produces a well known six-line spectrum. The whole velocity range is calibrated using these six velocity points. Naturally, any shifts in the spectra using this calibration are reported with respect to the zero point of  $\alpha$ -Fe

spectrum). The shape of the absorption spectrum was fitted to a theoretical model line shape, which was a superposition of singlets, doublets and sextets ( $^{57}\text{Fe}$  case) of a Lorentzian form. This was done with the aid of specialized computer programs. The result was investigated by chi 2 criterion and the theoretical line shape is tailored to fit the experimental spectrum by the adjustment of spectral parameters like isomer shift, quadrupole splitting, hyperfine magnetic field, *etc.*

For the magnetic measurements, a plastic drinking straw was used as the sample holder. A small portion of each sample, approximately 5-10 mg, was loaded into the straw. The magnetic moment of the sample was measured at room temperature in a commercial magnetometer (Quantum Design PPMS system), which is a Faraday-extraction type magnetometer. At each field value, 10 scans were measured and averaged.

## S2.1 Microwave heating analysis

The magnetic epoxy nanocomposite samples were sandwiched between the two SiC foams, and arranged as a packed bed reactor set-up, Scheme S1. This packed bed reactor set-up was then enclosed in the fused quartz tubing and irradiated at a fixed microwave power, with a constant flow of carrier gas ( $\text{H}_2/\text{Ar}$  mixture) flowing throughout the packed bed reactor. The average microwave power absorption value or the heating potential depends on the dielectric properties of the material, frequency of the microwave, and the electric field intensity,<sup>2-6</sup> which is given by Equation (S1):

$$Q_{avg} = \omega \cdot \epsilon_0 \cdot \epsilon'' \cdot E_{rms}^2 \quad (\text{S1})$$

where  $Q_{avg}$  is the average microwave power absorption or the heating potential in  $\text{W}/\text{m}^3$ ,  $\omega$  is the angular frequency rad/sec,  $\epsilon_0$  is the permittivity of free space ( $8.85 \times 10^{-12}$  F/m),  $\epsilon''$  is the relative dielectric loss factor of the absorbing media, and  $E_{rms}$  is the electric field

intensity in V/m. It is to be pointed out here that the dielectric loss factor indicates the ability of a microwave absorbing material to convert the absorbed microwave energy to heat energy, which in-turn depends on the temperature of the absorbing media. In the absence of  $\varepsilon''$  measurement of the material at different temperatures, Equation (S1) could be combined with the sensible heat of the absorbing media per unit time<sup>4</sup> and can be represented in a differential form, Equation (S2):

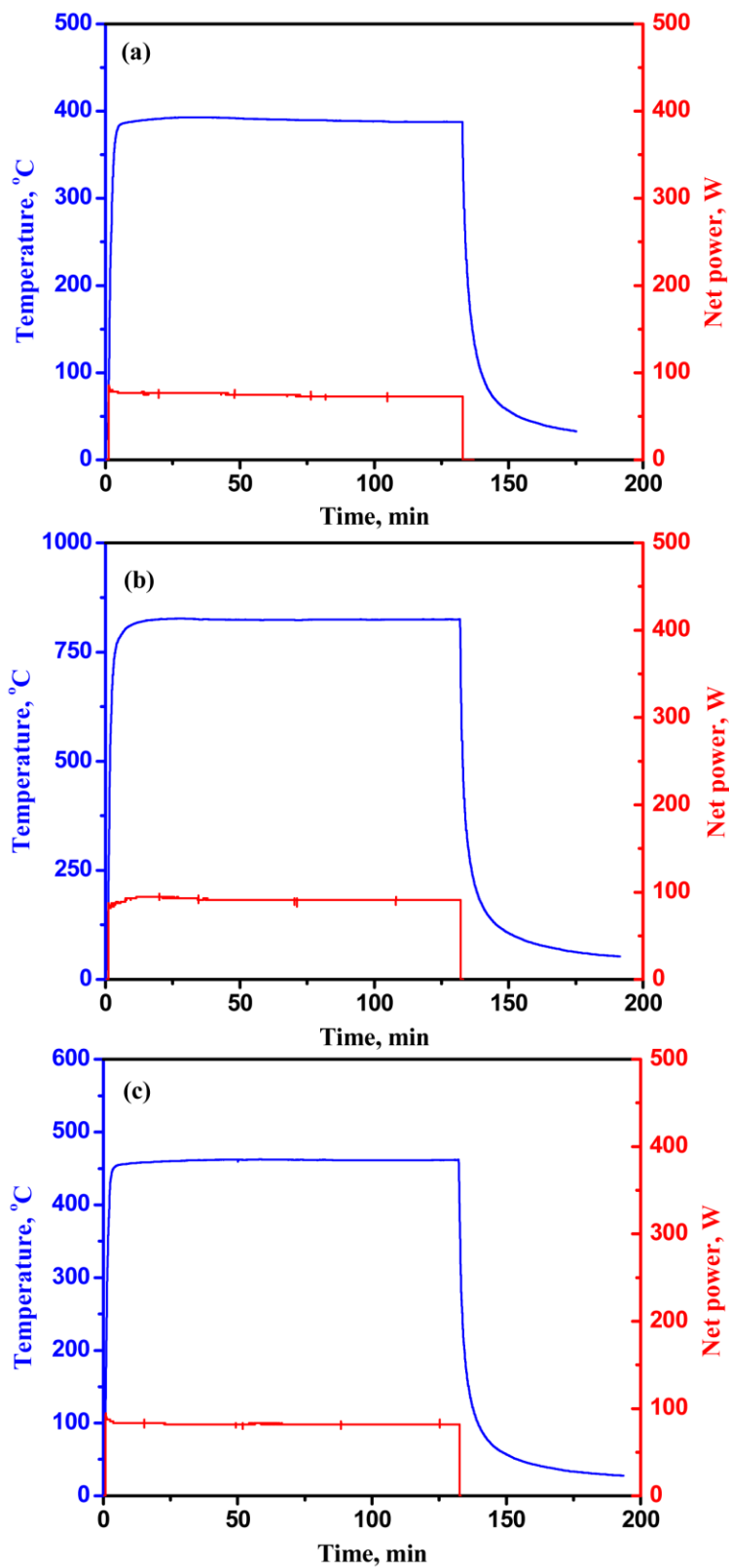
$$\left(\frac{d\varepsilon''}{dT}\right) = [\rho \cdot C_p / \omega \cdot \varepsilon_0 \cdot E_{rms}^2] \cdot \frac{d[\Delta T / \Delta t]}{dT} \quad (S2)$$

where  $\rho$  is the density of the absorbing media in kg/m<sup>3</sup>,  $C_p$  is the heat capacity of the absorbing media in J/kg·°C,  $\Delta T$  is the temperature change in °C, and  $\Delta t$  is the time interval in seconds.

Bulk surface temperature and net power profiles at three different purging gas rates, 20, 40 and 60 cc/min, were monitored and recorded as shown in Fig. S1. It is evident that all the temperature and power profiles follow a similar pattern, which can be divided into three regions: (1) sharp rise of bulk surface temperature and net power after turning on microwave (2) stabilization of temperature and power level at high within several minutes of operation (3) rapid decay of bulk surface temperature after turning off the microwave power. Fig. S1(a) shows the temperature and net power profile at a purge gas flow rate of 20 cc/min, where the bulk temperature stabilizes at ~390 °C with a net power of 74.5 W. With the increase in the gas flow rate to 40 cc/min, as shown in Fig. S1(b), the temperature jumps to 823 °C within a similar period of operation, with the net power increased to ~90.0 W. However, with the increase in the gas flow rate to 60 cc/min, as shown in Fig. S1(c), the bulk temperature surprisingly drops to 462 °C with a net power of 82.0 W. All these experimental runs reveal that the net power was well

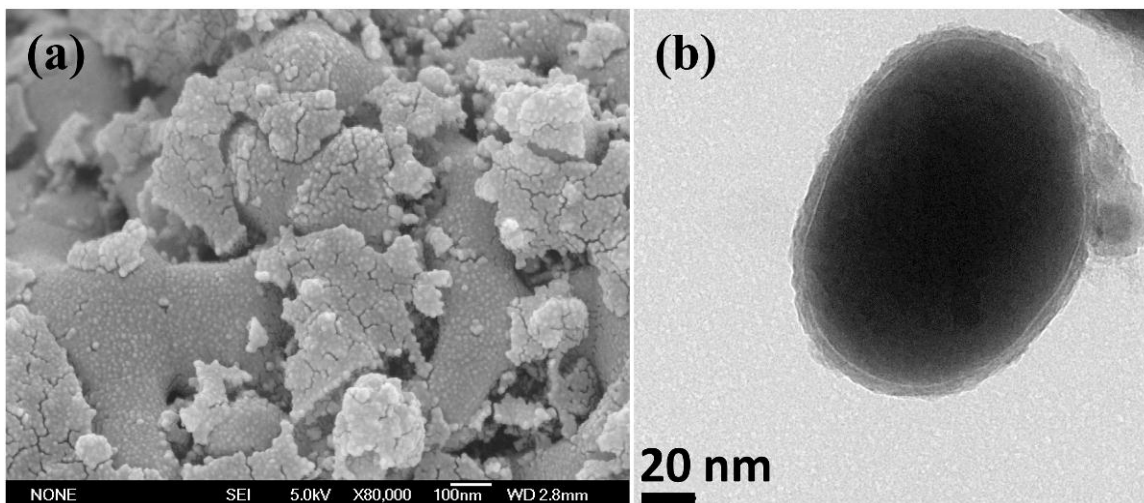
controlled within the range of 74.5-90.0 W, while the bulk temperature differs a lot at different purging gas flow rates. The much higher temperature obtained at 40 cc/min implies greater decomposition of the polymer sample, which in-turn generates large amounts of heat and possibly contributing to the temperature jump. At the same time, large purging gas flow rate (60 cc/min) also carries more heat out of the system and thus cools down the whole system.

Theoretically, the dielectric properties of the absorbing media is dependent on the frequency of the microwave energy being irradiated, and physical properties of the absorbing media such as temperature, density, mass, and specific heat capacity. With the frequency of the microwave energy irradiating the packed bed reactor configuration fixed, and all other factors being kept constant, the extent to which the absorbing media absorbs the irradiated microwave energy purely becomes a function of the mass of the absorbing media and its temperature as well as the carrier gas flow-rate. In our experimental runs, the net available microwave power for the absorbing media was maintained relatively constant during the entire duration of the experiment.

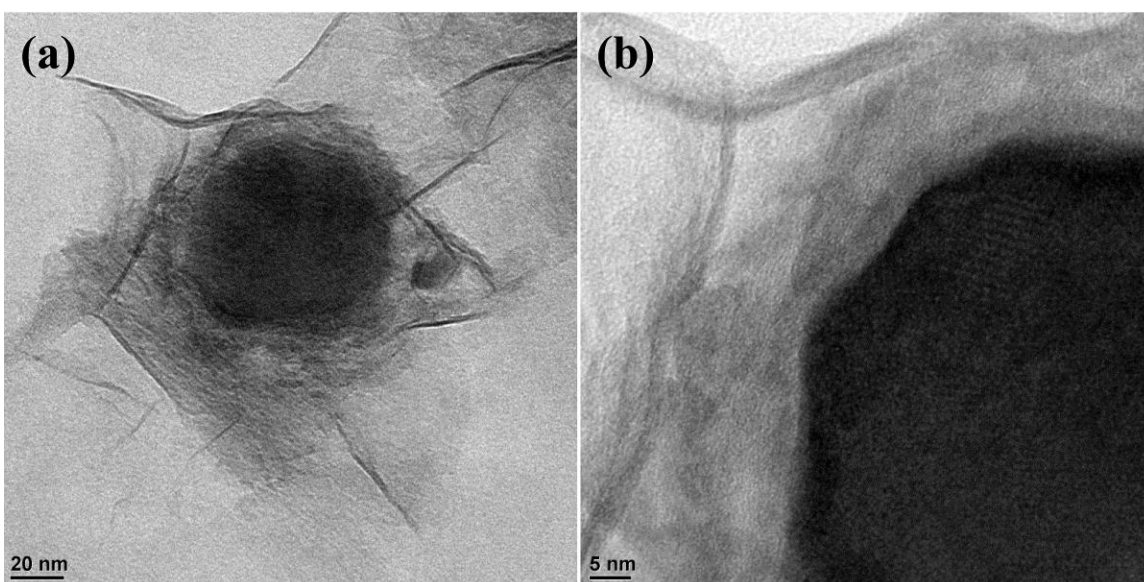


**Fig. S1** The temperature and net power profiles of epoxy nanocomposite samples with a purging gas rate of (a) 20 cc/min, (b) 40 cc/min, and (c) 60 cc/min.

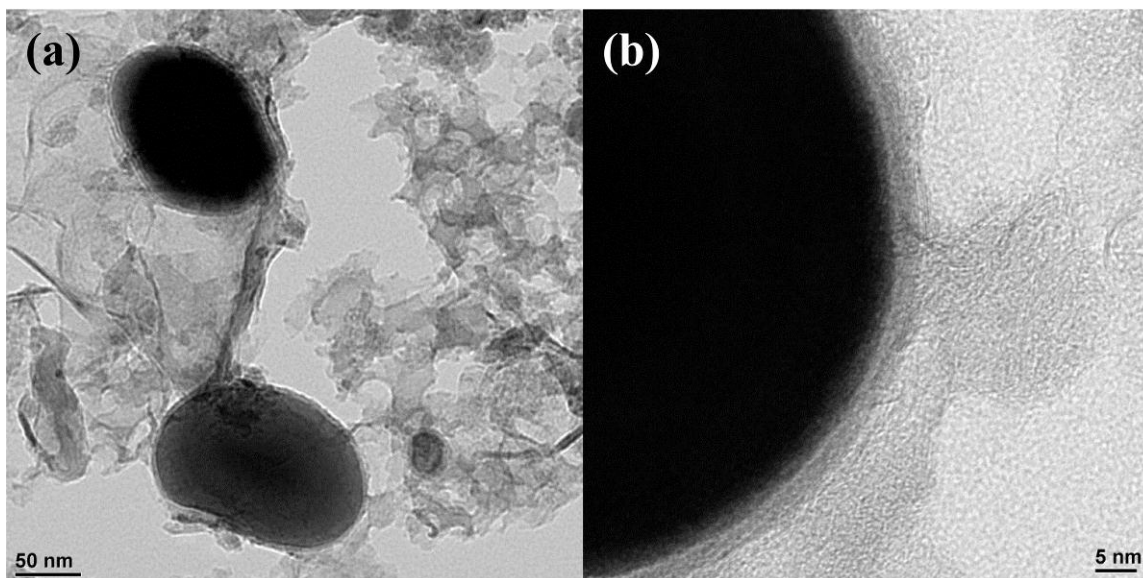
## S2.2. Microstructure of M20, M40, M60 and C60



**Fig. S2** (a) SEM and (b) TEM of M20.

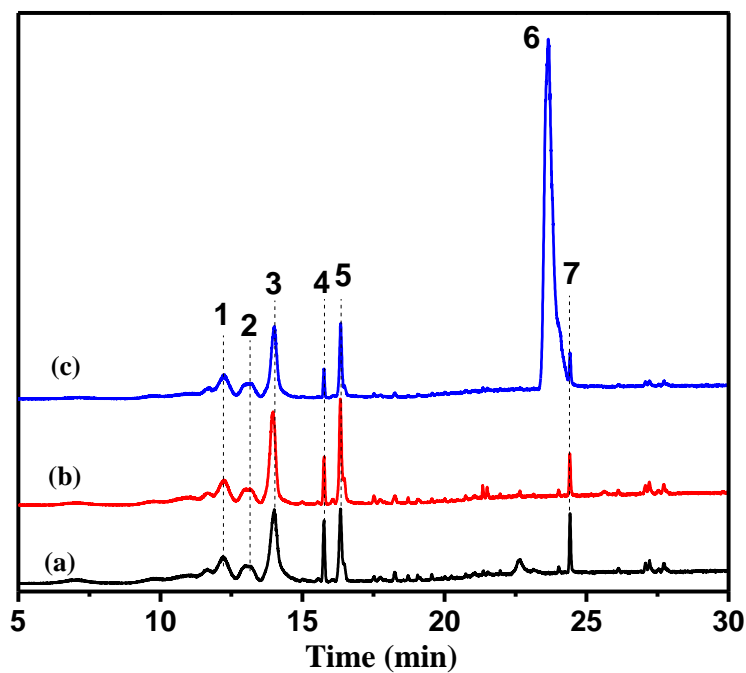


**Fig. S3** (a) TEM of M40 and (b) enlarged area at the interface.



**Fig. S4** (a) TEM of M60 and (b) enlarged area at the interface.

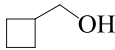
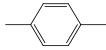
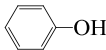
### S2.3 GC-MS analysis of degradation gas species



**Fig. S5** GC-MS of gas species degraded from epoxy nanocomposites at the purging gas rate of (a) 20 cc/min, G20, (b) 40 cc/min, G40, and (c) 60 cc/min, G60.

The major degraded gas species after applying different flow rates of purging gas were analyzed by gas chromatography/mass spectrometry (GC/MS). The gas species are simply noted as G20, G40 and G60 at the gas flow rates of 20, 40 and 60 cc/min, respectively. Table S1 exhibits the assigned seven structures for each peak from No.1 to No. 7 in Fig. S5. The structures were identified through the analysis of the mass fragmentation patterns as compared to the standard patterns of pure chemical compounds. The gas compounds obtained from different purging gas flow rates were observed to be the same with a significant difference in the fraction, Table S1. Seven main peaks are observed, dodecane (m/z 170), hexadecane (m/z 226), toluene (m/z 92), cyclobutanemethanol (m/z 86), p-xylene (m/z 106), phenol (m/z 94) and benzofuran(m/z 118).

**Table S1.** The gas species degraded from G20, G40 and G60.

No	Species	Structure	G20 (%)	G40 (%)	G60 (%)
1	Dodecane		19.4	19.0	5.2
2	Hexadecane		7.1	6.1	3.1
3	Toluene		21.4	23.1	10.2
4	Cyclobutanemethanol		3.8	3.0	0.9
5	p-Xylene		8.3	13.1	5.0
6	Phenol		/	/	66.8
7	Benzofuran		11.4	10.8	2.6

## S2.4 Selected area electron diffraction (SAED) analysis

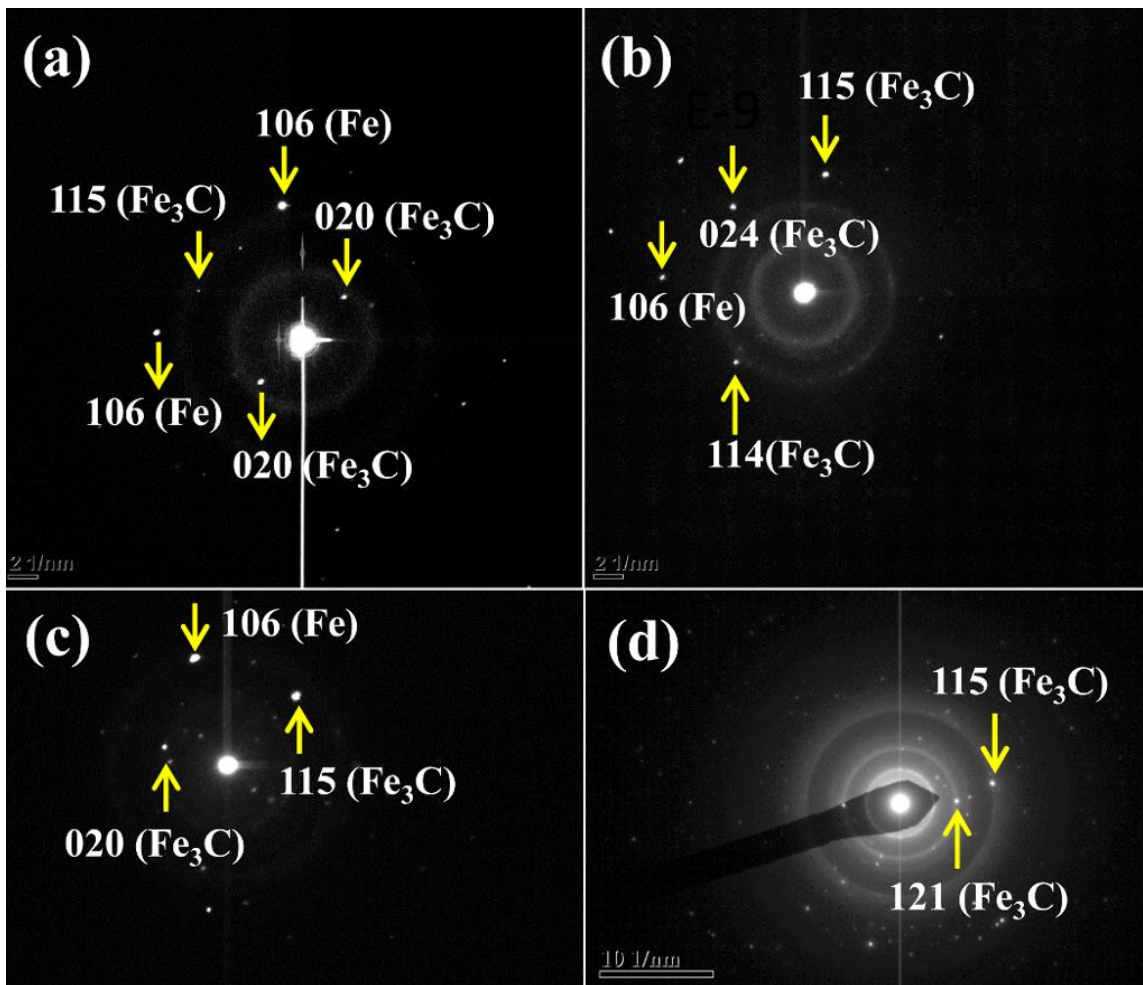
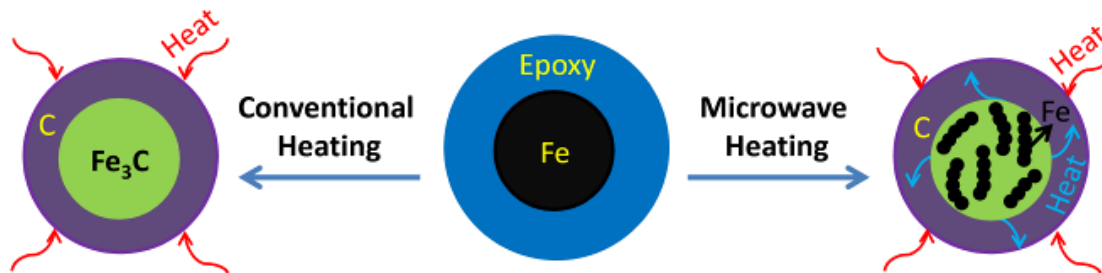
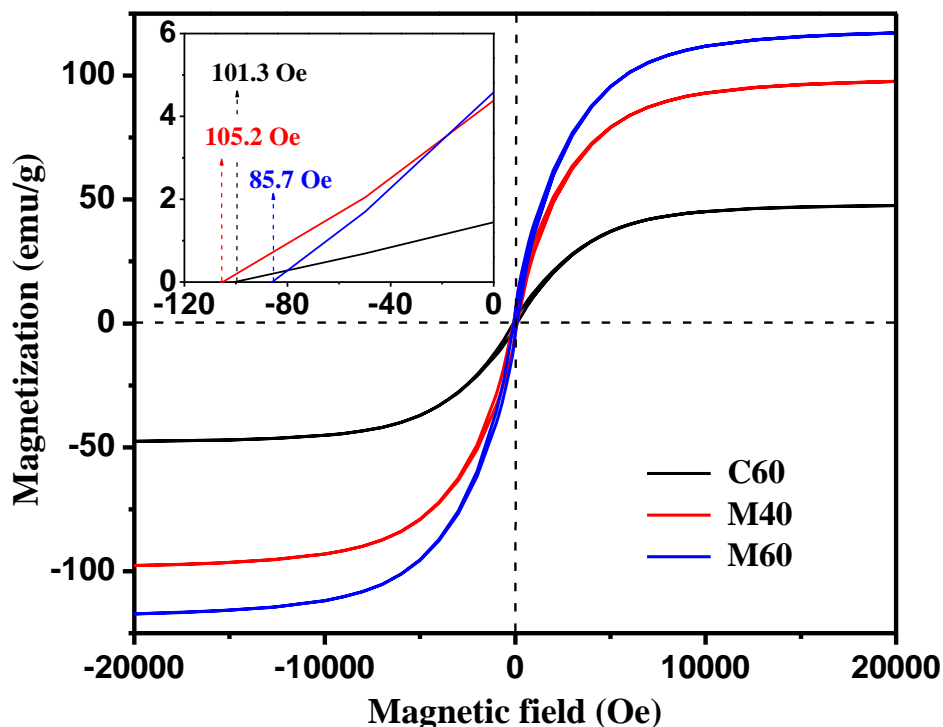


Fig. S6 SAED analysis of M20, M40, M60 and C60.



Scheme S2 Comparison of conventional and microwave pyrolysis on nanoparticle microstructure formation.

## S2.5 Magnetic property



**Fig. S7** Room temperature magnetic hysteresis loops of C60, M40 and M60.

Fig. S7 shows the room temperature hysteresis loop of the core-shell NPs after microwave and conventional annealing. These three samples are comparatively investigated because C60 and M40 have a similar annealing temperature while C60 and M60 used the same gas flow rate. Apparently, the saturation magnetization ( $M_s$ ) of the core-shell nanoparticles from microwave annealing (M40 and M60) are significantly higher than that of the one annealed from a conventional approach (C60). C60 exhibits a relatively small  $M_s$  of 47.6 emu/g, while M40 and M60 show more than doubled  $M_s$  of 97.8 and 117.2 emu/g, respectively. The higher  $M_s$  of the microwave annealed samples is due to the existence of metallic Fe within the magnetic core, which acquires much higher  $M_s$  value of 220 emu/g<sup>7</sup> as compared to Fe<sub>3</sub>C (the  $M_s$  for bulk Fe<sub>3</sub>C is 130 emu/g<sup>8</sup>). Once the specific component of magnetic species has been revealed by Mössbauer spectra, the fraction of magnetic core and carbon could be determined using the magnetization values.

Even though thermogravimetric analysis is a useful tool to determine the weight fraction of each component, it is hard to precisely analyze the component fraction in this case since the oxidation of magnetic core will bring the weight up and the weight loss of carbon degradation appears within the same temperature region. Therefore, it is very hard to distinguish how much carbon is degraded on an upward weight percentage curve, Fig. S8. However, it is possible to estimate the weight fraction of magnetic core and carbon substrate from  $M_s$  value of each sample. Specifically, the weight fraction of  $\text{Fe}_3\text{C}$  in C60 can be calculated to be 36.6% ( $47.6/130=0.366$ ) and the rest carbon is 63.4%. In M40 and M60, the  $M_s$  of the magnetic core is the summation of two components, namely Fe and  $\text{Fe}_3\text{C}$ , each component times their specified weight fraction, which is determined from Mössbauer spectra. As a result, the  $M_s$  of magnetic core in M40 and M60 is calculated to be 153.4 and 156.1 emu/g and their weight fraction is estimated to be 63.8 and 75.1 %, respectively. The larger fraction of magnetic core in M40 and M60 compared to C60 indicates that the microwave annealing is beneficial for deeper degradation of epoxy nanocomposites into volatiles. In addition, larger purging gas rate also helps to decompose the epoxy more completely. The inset of Fig. S7 shows the coercivity ( $H_c$ ) of each sample, which is located near 100 Oe, revealing soft ferromagnetic cores.

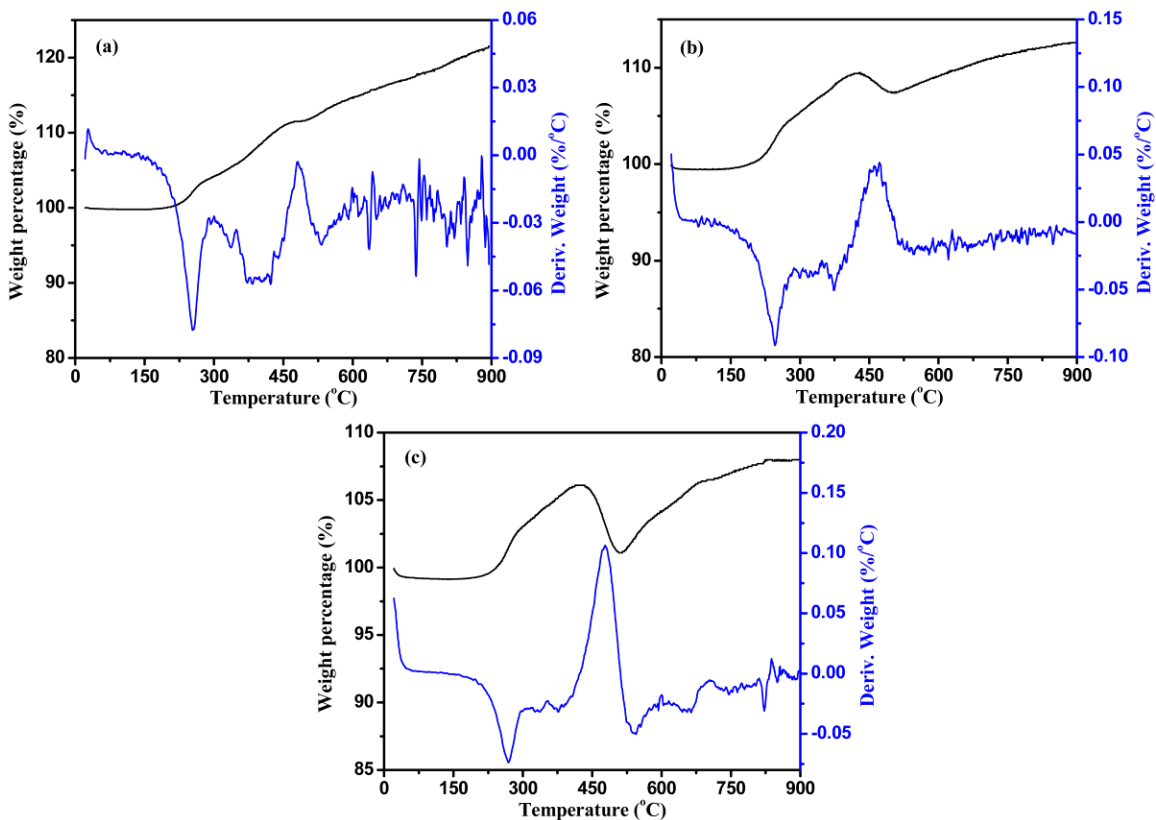


**Fig. S8** TGA and derivative weight curve of (a) M20, (b) M40 and (c) M60.

## S2.6 Mechanism of different carbon nanostructure formation

The carbon nanotube growth mechanism follows a base-<sup>9</sup> rather than tip-<sup>10</sup> growth model since the catalyst particles are not observed at the tip or middle of the tube. For the carbon nanoflakes, the highest temperature around 800 °C allows the space structure of the orbitals of a free carbon atom to be asymmetric, with three in-plane  $sp^2$  bonds and one  $p_z$  orbital that perpendicular to this plane. Such a configuration has the potential to form a plane structure and is native for the asymmetric surface energy of graphite. This asymmetric factor has proven to be important for the formation of carbon nanoflakes.<sup>11</sup> The amorphous and graphitized carbon shell formation is similar, where the polymer is carbonized and deposited on the nanoparticle surface. The deposited carbon is going to be graphitized at high temperature such as 800 °C in a conventional process while it

maintained amorphous at relatively lower temperature such as 450 °C in microwave assisted process at the gas flow rate of 60 cc/min.

### S3. References

1. J. Zhu, S. Wei, J. Ryu, L. Sun, Z. Luo and Z. Guo, *ACS Applied Materials & Interfaces*, 2010, **2**, 2100-2107.
2. I. Plazl, G. Pipus and T. Koloini, *AIChE Journal*, 1997, **43**, 754-760.
3. A. C. Metaxas and R. J. Meredith, eds., *Industrial Microwave Heating.*, Power Engineering Series 4, London, UK, 1983.
4. Z. Hashisho, M. Rood and L. Botich, *Environmental Science & Technology*, 2005, **39**, 6851-6859.
5. M. D. Turner, R. L. Laurence, W. C. Conner and K. S. Yngvesson, *AIChE Journal*, 2000, **46**, 758-768.
6. T. Ohgushi, Y. Sakai, Y. Adachi and H. Satoh, *The Journal of Physical Chemistry C*, 2009, **113**, 8206-8210.
7. J. Zhu, H. Gu, S. B. Rapole, Z. Luo, S. Pallavkar, N. Haldolaarachchige, T. J. Benson, T. C. Ho, J. Hopper, D. P. Young, S. Wei and Z. Guo, *RSC Advances*, 2012, **2**, 4844-4856.
8. I. Morjan, R. Alexandrescu, M. Scarisoreanu, C. Fleaca, F. Dumitrache, I. Soare, E. Popovici, L. Gavrilă, E. Vasile, V. Ciupina and N. C. Popa, *Applied Surface Science*, 2009, **255**, 9638-9642.
9. L. J. Ci, Z. G. Zhao and J. B. Bai, *Carbon*, 2005, **43**, 883-886.
10. S. Iijima, P. M. Ajayan and T. Ichihashi, *Physical Review Letters*, 1992, **69**, 3100-3103.
11. N. G. Shang, F. C. K. Au, X. M. Meng, C. S. Lee, I. Bello and S. T. Lee, *Chemical Physics Letters*, 2002, **358**, 187-191.